Arab J Geosci (2016) 9: 264
DOI 10.1007/s12517-015-2239-z

ORIGINAL PAPER

Stress analysis of NW Jordan: New episode of tectonic rejuvenation related to the Dead Sea transform fault

M. Alawabdeh[1] · J. V. Pérez-Peña[2,3] · J. M. Azañón[2,4] · G. Booth-Rea[2,4] · A. M. Abed[5] · M. Atallah[6] · J. P. Galve[2]

Received: 18 June 2015 / Accepted: 18 November 2015 / Published online: 28 March 2016

Abstract We performed a stress analysis based on fault-slip data for two of the main geological structures in NW Jordan; the Amman-Hallabat (AHF) and Shueib (SHF) faults. Both structures formed in Cretaceous times under E-W to ESE-WNW maximum compressive stress and have been considered inactive in Neogene and Quaternary times. We have collected data from 14 field stations in the area between the Dead Sea and the cities of Amman and Al Salt. This dataset comprises about 306 fault-slip data that include fault orientations and kinematics, striations, and joints. With the aid of the software T-TECTO 3.0, we have obtained the main stress axes for each station. Our results suggest that most of the structures are coherent with the present-day stress pattern associated with the Dead Sea fault system. In most of the field stations, new striations clearly overprint the older ones. Present-day stress field in the region has horizontal to sub-horizontal maximum and minimum compressive axes (σ1 and σ3), striking NNW-SSE and ENE-SWS, respectively, and a vertical intermediate stress axis (σ2). These new findings suggest a rejuvenation of the AHF and the SHF in the Quaternary in the context of the Dead Sea transform fault tectonic activity.

Keywords Stress analysis · Tectonic rejuvenation · Amman-Hallabat fault · Shueib fault · Dead Sea transform fault · Jordan

✉ M. Alawabdeh
moh.awabdeh@gmail.com

[1] Department of Natural and Chemical Resources, Faculty of Engineering, Tafila Technical University, Tafila, Jordan

[2] Facultad de Ciencias, Departamento de Geodinámica, Universidad de Granada, Campus de Fuentenueva, Avd. Fuentenueva, S/N, Granada 18071, Spain

[3] Instituto Andaluz de Geofísica, Universidad de Granada, Campus de Cartuja, 18071 Granada, Spain

[4] Instituto Andaluz de Ciencias de la Tierra, CSIC-UGR, Avd. Palmeras, 4, Armilla Granada, Spain

[5] Department of Geology and Environment, Jordan University, Amman, Jordan

[6] Department of Earth science, Al-Yarmouk University, Irbid, Jordan

Introduction

The Dead Sea transform fault (DSTF), with more than 1000 km of length, is the main active structure in the Middle East and forms the NW plate boundary between Arabia and Africa plates. The maximum compressive stress axis near the fault zone is horizontal with a NNW-SSE direction, while the minimum compressive stress is also horizontal, favoring NE-SW-directed extension in a general normal stress regime. The DSTF accommodates most of the crustal stress in the region (McClusky et al. 2003; Gòmez et al. 2007; Al-Tarazi et al. 2011) (Fig. 1a). However, other regional structures as the Syrian Arc System have been suggested to accommodate part of this stress (Chaimov et al. 1990; Badawy and Horváth 1999; Abou Romieh et al. 2009; Alchalbi et al. 2010). The Jordanian part of the latter arc system is partially composed of two main structures: the Amman-Hallabat Structure (AHS) and the Shueib Structure (SHS) (Mikbel and Zacher 1981; Diabat 2009) (Fig. 1b). Both structures are dextral fold-thrust belts formed in the Cretaceous under E-W to ESE-WNW maximum compressive stresses (Quennell 1959; Mikbel and Zacher 1981). They were considered inactive during the Neogene, but recent studies have proposed a Quaternary tectonic activity of these structures (Diabat 2009).

The AHS and the SHS are connected to the southern segment of the DSTF, the northern Wadi Araba Fault (WAF),

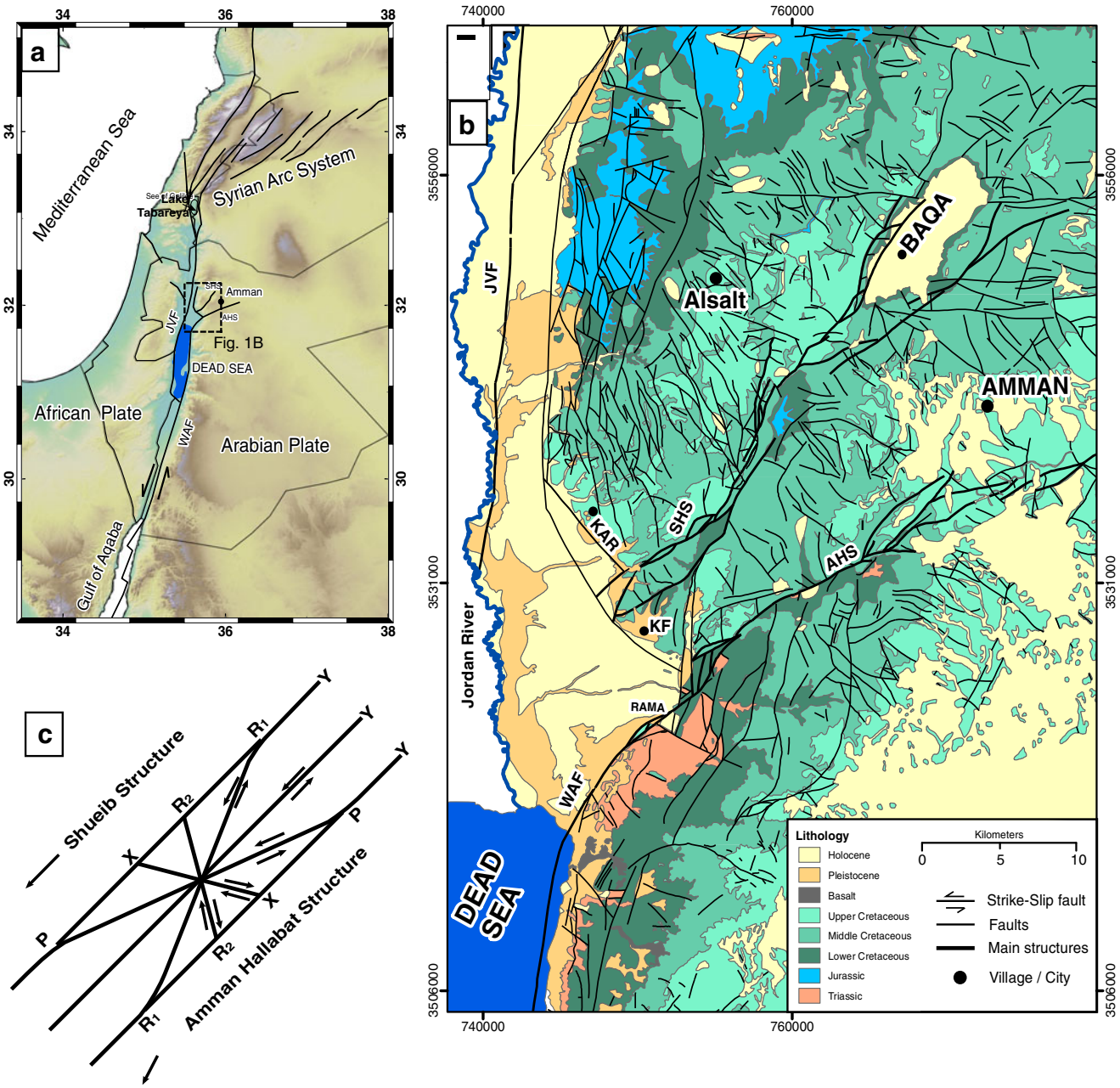

Fig. 1 **a** Regional tectonic context of the Dead Sea transform fault and the Syrian Arc System. The inset shows the location of the study area. **b** Geological map for the study area (NW Jordan). Main structures have been highlighted. *AHS* Amman-Hallabat Structure, *SHS* Shueib Structure, *WAF* Wadi Araba Fault, *JVF* Jordan Valley Fault, *KF* Kafrain village, *Kar* Karama village, *Rama* Rama village. **c** Reidel shear model of the study area and the orientation of the primary and secondary faults

but the stress fields associated with these two structures is not well constrained. Diabat (2009) presented a structural analysis of the northernmost part of the AHS in the Amman area and proposed that the stress field orientation related to the AHS was similar to the regional one associated with the DSTF. However, the relation between the AHS and SHS with the present-day activity of the DSTF has not been analyzed further.

In this work we conducted a field campaign to collect fault-slip data in order to perform a detailed structural and paleostress analysis for the AHS and SHS. The structural analysis is based on 14 field stations with 306 data of fault planes and slickensides. We used the T-TECTO 3.0 software for analyzing structural data (Zalohar 2009). Besides this analysis, we documented field outcrops proving the multi-phased stress field registered in the region that affects the AHF and SHF structures. We have compared the results of the structural analysis with seismological data (Hofstetter et al. 2007; Palano et al. 2013) and results of previous paleostress

analyses (Zain Eldeen et al. 2002; Diabat et al. 2004; Diabat 2009; Hardy et al. 2010). This structural analysis suggests that the AHS and SHS faults are being affected by a stress pattern compatible with the DSFT field stress.

Geological and tectonic setting

Stratigraphy

The study area presents geological formations from Triassic to Holocene (Fig. 1b). The oldest formations (Triassic) are mostly composed of sandstone with sandy limestone and dolomite (Makhlouf 2003). The Jurassic formations crop out in the NW part of the study area and comprise seven units: Hihi Claystone Formation, Nimir Limestone Formation, Silal Sandstone Formation, Dahab Limestone Formation, Ramla Sandstone Formation, Hamam Sandstone Formation, and Mughanyya Limestone Formation (Masri 1963; Abed 2000). Most of the rocks from the study area are Cretaceous. The Lower Cretaceous units are pure sandstones, and the Middle-Upper Cretaceous units are limestones with marl. These Cretaceous rocks are sealed by silicified limestone and chert (Powell 1989). Only one formation belongs to the Paleogene, composed mainly of chert (Abed 2000) and crops out away from the AHS and the SHS.

Neogene and Pleistocene sediments were largely removed by erosion, and only two Quaternary formations can be identified in the study area, the Lisan and Damya formations. The estimated age of the Lisan formation is 70–14 ka (Abed and Yaghan 2000; Landmann et al. 2002; Hasse-Schramm et al. 2004). The age attributed to the Damya formation is 15–12 ka (Abed and Yaghan 2000) and is composed of reddish evaporate-free sediments. The Lisan and Damya formations occur in restricted areas of the Jordan Valley and the Dead Sea. The overlaying thin layers of soil and colluvial sediments are distributed in the Wadis and scattered areas. The age of the formations and detailed descriptions of the stratigraphy are summarized in Table 1.

Tectonic setting

The Red Sea opening and the collision of the Arabia and Eurasian plates are the main mechanisms determining the stress field in northwestern Arabia (Al-Tarazi et al. 2011; Reilinger and McClusky 2011). The stress field in northwestern Arabia is produced by this movement that occurs along one of the largest transform faults in the world, the DSTF. The DSTF has two main segments, the northern one extending from the Lake Tabareya to Taurus and the southern segment from the Gulf of Aqaba to the Lake Tabareya (Al-Tarazi et al. 2011). The southern segment has, in turn, two main faults; the Wadi Araba Fault (WAF) and the Jordan Valley Fault (JVF) (Ferry et al. 2007; Le Beon et al. 2010).

The WAF is almost pure-sinistral strike-slip composed of several linear segments tens of kilometers long connected either by compressive or extensive jogs that form small-scale push-up ridges and pull-apart basins (Garfunkel 1981; Atallah 1992; Klinger et al. 2000; Hofstetter et al. 2007; Le Beon et al. 2008, 2010). In its northern termination, the WAF strikes NE forming a restraining bend with a major reverse component together with the sinistral sense of movement.

Apart of the WAF in the NE of the Dead Sea, geological structures such as the AHS and the SHS show inherited Cretaceous deformation related to the central Syrian Arc System (Mikbel and Zacher 1981). Both structures are believed to form under a tectonic frame of NW-SE maximum compressive stress forming the NE-SW dextral-reverse faults and the parallel folds in the Late Cretaceous (Mikbel 1986; Diabat 2009). The AHS extends about 80 km from the northeastern corner of the Dead Sea to Qaser Al Hallabat (Arabic name for Alhallabat Palace), while the SHS extends from the Kafrain dam to Zarqa River with a total length of 45 km. Diabat (2009) obtained several structural data taken from quarries in the city of Amman and proposed a possible reactivation of the northernmost part of the AHS in Quaternary times. Similar to the AHS, the SHS is formed by antithetic and synthetic dextral small reverse and dextral strike-slip faults (Mikbel and Zacher 1981). It extends from the west of Al-Kafrain village (25 southwest Amman) to the north of Al-Baqa (Fig. 1). The SHS was though to remain inactive since the time of its formation, but a recent study has proposed a Quaternary activity for this structure.

Stress fields of the DSTF, the AHS, and the SHS

Several studies have analyzed the stress fields in the region under the light of the deformation accommodated by the DSTF (e.g., Eyal et al. 2001; Zain Eldeen et al. 2002; Diabat et al. 2004; Diabat 2009; Hardy et al. 2010; Homberg and Bachmann 2010). Likewise, the studies presented by Hofstetter et al. (2007) and Palano et al. (2013) highlight the current stress regime through seismicity and GPS data analysis. Most of the published works agree to assign a NNW-SSE horizontal maximum compressive stress ($\sigma 1$) and an ENE-WSW horizontal minimum compressive stress ($\sigma 3$) in the Dead Sea area (Hofstetter et al. 2007; Diabat 2009; Hardy et al. 2010). By contrary, there are few studies about the AHS and the SHS structures (Quennell 1959; Mikbel and Zacher 1981; Mikbel 1986; Diabat 2009).

Methodology

The objective of this work is to evaluate and determine the Quaternary tectonic stress from the fault-slip data measured in the AHS, the SHS and the northern WAF. Prior to the field

Table 1 Details of the litho-stratigraphy of the study area

Age		Group	Formation (Masri 1963)	Formation (Powell 1989)	Formation (Abed 2000)	Lithology
Quaternary	L. Pleistocene-Holocene				Damya	Fluvial sediments
	Pleistocene				Lisan	Gypsum, aragonite and sands
Paleogene	Eocene	Belqa	Muwaqqar	Um Rijam		Chert
	Paleocene			Muwaqqar		Chalk
L. Cretaceous	Maastrichtian		Ammam	Alhisa		Phosphorite/oyster
	Campanian			Amman Silicified		Chert interbeded with silicified
				limestone		limestone.
				Gudran		Chalk
	Santonian		Gudran	Wadi Es-sir		Massive limestone
	Coniacian	Ajlun		Shuayb		Limestone and marl
	Turonian		Wadi Es-Sir	Hummar		Limestone
				Fuheis		Marl
			Shuieb			Marl and limestone
	Cenomanian		Hummar		F/S/H	Limestone
			Fuheis			Marl
			Naur			Limestone
E. Cretaceous	Albian	Kurnub	Baqa	Subeihi		Fluvial and marine sandstone
M. Jurassic	Callovian					
		Azab			Azab	Sandy dolomitic limestone
	Bathonian					
M. Triassic	Ladinian				Irak El-Amir	Dolo. lim, limestone and marl
	Ladi - Anis				Mukheiris	Sandstone with Marly shale
	Ramtha					
	Anisian				Hisban	Dolomitic limestone
E. Triassic	Olenekian ?				Ein Musa	Shale, Marl and fine sandstone

work, aerial photographs of the study area were analyzed for the initial identification of potential areas with active or recent fault outcrops. These aerial photos also assisted to validate the (1:50,000) geological sheet maps published by the Natural Resources Authority in Jordan. We used a Digital Elevation Model (DEM) of 30 m resolution to derive a hillshade base map for the field station map. This DEM was downloaded from the Advanced Spaceborne Thermal Emission and Reflection Radiometer (ASTER) Global Elevation Model (GDEM) website (http://www.gdem.aster.ersdac.or.jp/ASTER_GDEM).

Structural data consist of 306 measurements of faults and slickensides collected from 14 field stations. Field data were measured using the Freiburg equivalent compass (Krant Geological Structural 360°) which facilitates measuring the dip and strike in one operation by a vertical circle at the lid hinge. The location of the field stations were measured using a Garmin eTrex Vista HCx G.P.S. with an accuracy of less than 10 m. We focused the field work on the outcrops of the major fault zones where these structures experienced different phases of deformation (highlighted in Figs. 1 and 5). Most of the measurements were collected from middle-late Cretaceous formations, and a few of them were collected from Neogene and Quaternary rocks. These formations are mostly Carbonate rock formations that show clear striations and/or slicken fibers on the fault planes (Figs. 2 and 3).

We conducted field and mechanical analysis of meso-scale faults. We focused on meso-scale faults because in multi-phased deformations, like in our study, large-scale faults often underwent big displacements (Angelier 1994; Hardy et al. 2010). In such cases, first slip movement can be difficult to identify, especially if the fault reactivates under a different stress field and the new slip overprints the old slickensides. Conversely, in small and meso-scale faults, common in the study area, multiple slickensides can be preserved easier.

Different methods for stress analysis have been developed from the concept of stress inversion (Wallace 1951; Bott 1959; Angelier 1989, 1990, 1994; Delvaux 1993, 2011; Delvaux et al. 1995; Zalohar and Verbac 2007; Zalohar 2012). Our analysis was performed using the "T-TECTO 3.0 Professional" software for structural analysis (Zalohar 2009).

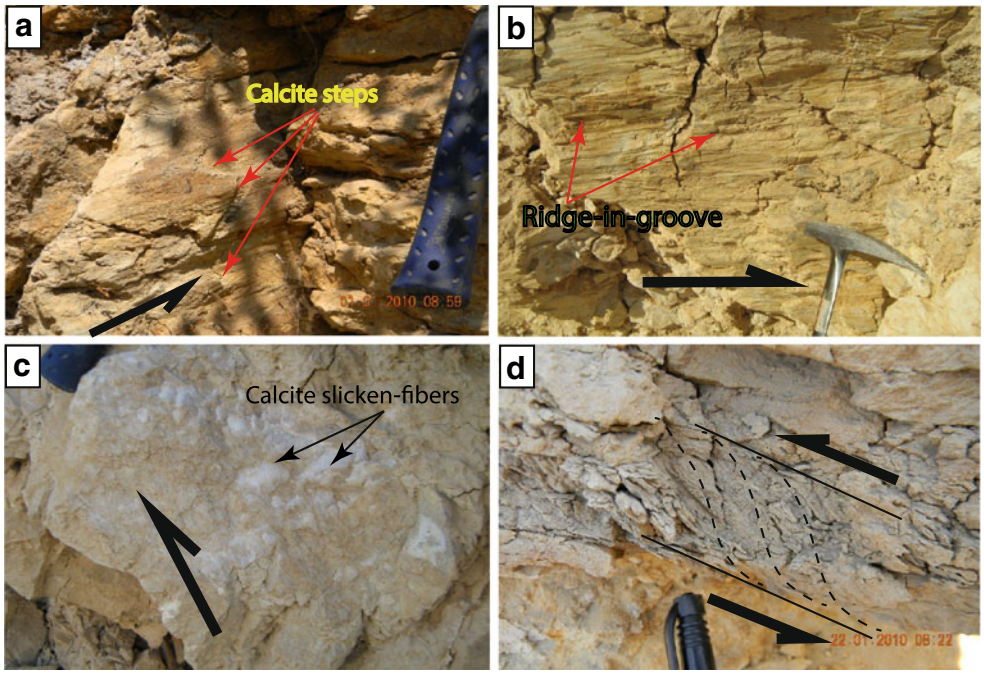

Fig. 2 Different movement indicators along fault planes in the study area; slickensides and slicken fibers (**a**, **b**, **c**), "*C-S*" structures in faulted sandstone layers (**d**)

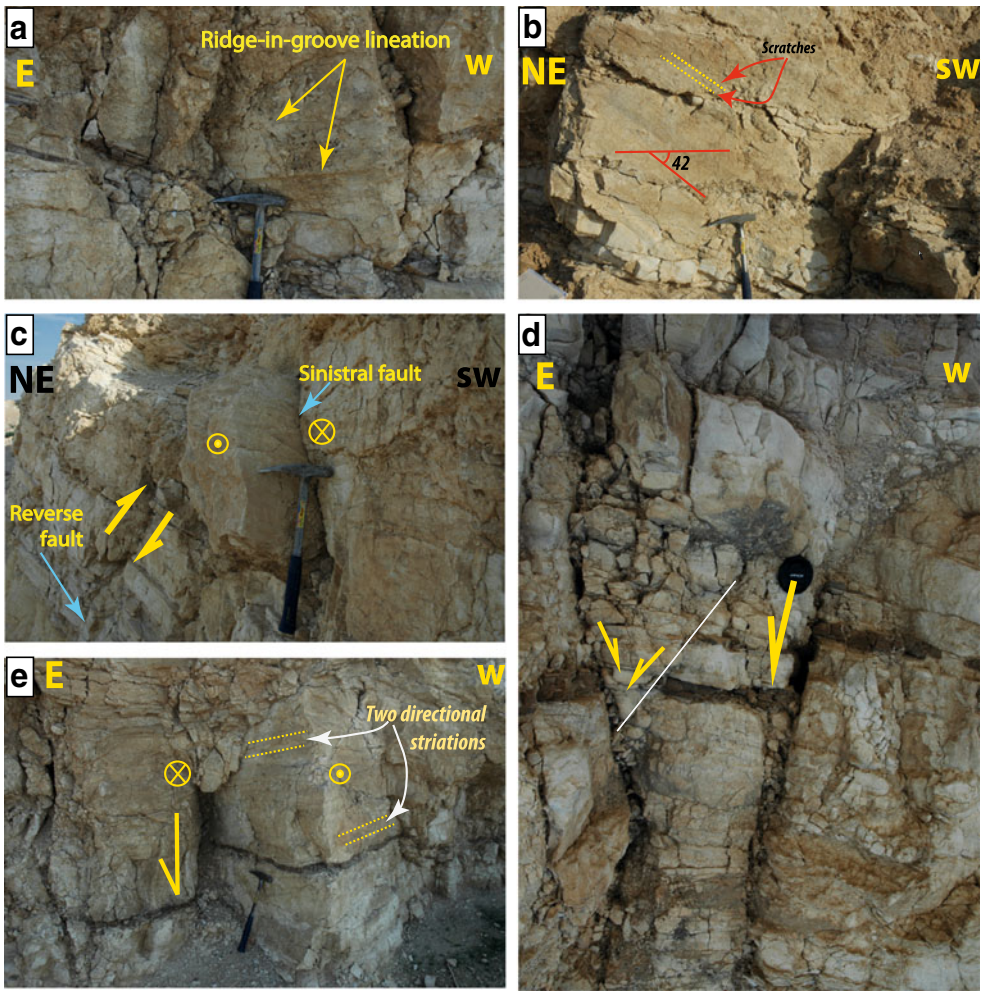

Fig. 3 Field outcrops of the station number 2. *Yellow dotted lines* indicate the direction of the slickensides. **a** Sinistral strike-slip fault in NW-SE direction. **b** Vertical fault of oblique sinistral-thrust in NE-SW direction. **c** Sinistral strike-slip fault adjacent to reverse-sinistral fault. **d** Highly fractured block, two small normal faults (*displacement of the brown thin chert layer*). **e** Double movements of normal and strike-slip faults perpendicular to NE-SW sinistral strike-slip fault

We used the Gauss Method associated with the visualization of P and T dihedra (Zalohar and verbac 2007). This method allows analyzing a mixture of various field data (fault plane measurement, joints, open fractures, veins, disjunctive foliation, and cleavage). The resulting stress tensor obtained from this method shows compressive and extension fields of the ellipsoid in red and blue colors, respectively. The virtual stress axes of the tensor are shown in red and blue arrows over a lower-hemisphere projection (Fig. 4). The results of the stress-inversion estimate the orientation of the three principle stresses (σ1, σ2, and σ3); where σ1 is the maximum compressive stress, σ2 is the intermediate compressive stress, and σ3 is the minimum compressive stress. The stress ratio is defined as $D=(\sigma2-\sigma3)/(\sigma1-\sigma3)$.

Analysis of field structural data

The bulk data of the field stations comprise two main trends of faults planes and fault traces traceable in the geological map (Figs. 5 and 6). The faults measurements used in our study area are meso-scaled faults (Figs. 3, 7, and 8). Since the stress field implies a variety of fractures/faults scales, these faults reflect the same mechanisms as the large-scale faulting. The fault types were mainly NE-SW oblique reverse and NW-SE normal faults. Less abundant, left and right strike-slip faults were measured striking N-S and NNW-SEE, respectively. The slip direction of the faults was determined using slickensides and calcite and/or gypsum fibers on fault planes (Fig. 2). Sense of slip indicators include tails and scratches as well as crescent marks formed by the intersection of the main fault plane with secondary fractures such as: R1, R2, X, and T (Figs. 1c and 2).

Field observations in the southern part of the study area and near to the Dead Sea show 30–40° trending left-lateral strike-slip faults cutting Quaternary deposits (Fig. 1b, c). The sense of movement of these faults is oblique sinistral with a NE reverse component (Fig. 3). Different phases of faulting are attested in some fault planes by the presence of multiple slickensides. Dip-slip striations are overprinted by strike-slip slickensides and calcite fibers, thus suggesting the reactivation of these faults (Figs. 3 and 7). The normal faults found in most stations strike in the range of N 110° E to N 170° E (clockwise sense) (Fig. 8). Their dips generally exceed 55°, the majority of them dipping between 65° and 90°.

The location and details of the 14 stations with the calculated paleostress ellipsoids are shown in Fig. 5 and Table 2. We have classified the obtained stress tensors into three categories: strike-slip, normal, and thrust tensors. Strike-slip stress tensors have the maximum (σ1) and minimum (σ3) stress axes sub-horizontal and the intermediate axis (σ2) sub-vertical. Normal stress tensors present σ1 sub-vertical and sub-horizontal σ3 and σ2. Thrust stress tensors have σ1 and σ2 sub-horizontal and σ3 sub-vertical. The strike-slip tensors were found in two forms; pure strike-slip and reverse strike-slip. Pure strike-slip tensors were found in 6 field stations (5, 6, 7, 10, 12, and 14) while the inverse component was identified in 4 stations (1, 8, 11, and 13). Generally, most of these stations spread over the main faults of the AHS and the SHS, and only one is located in the WAF area (Fig. 5). Left-lateral strike-slip faults strike N-S and run parallel to the DSTF. Thrust tensors were found in field

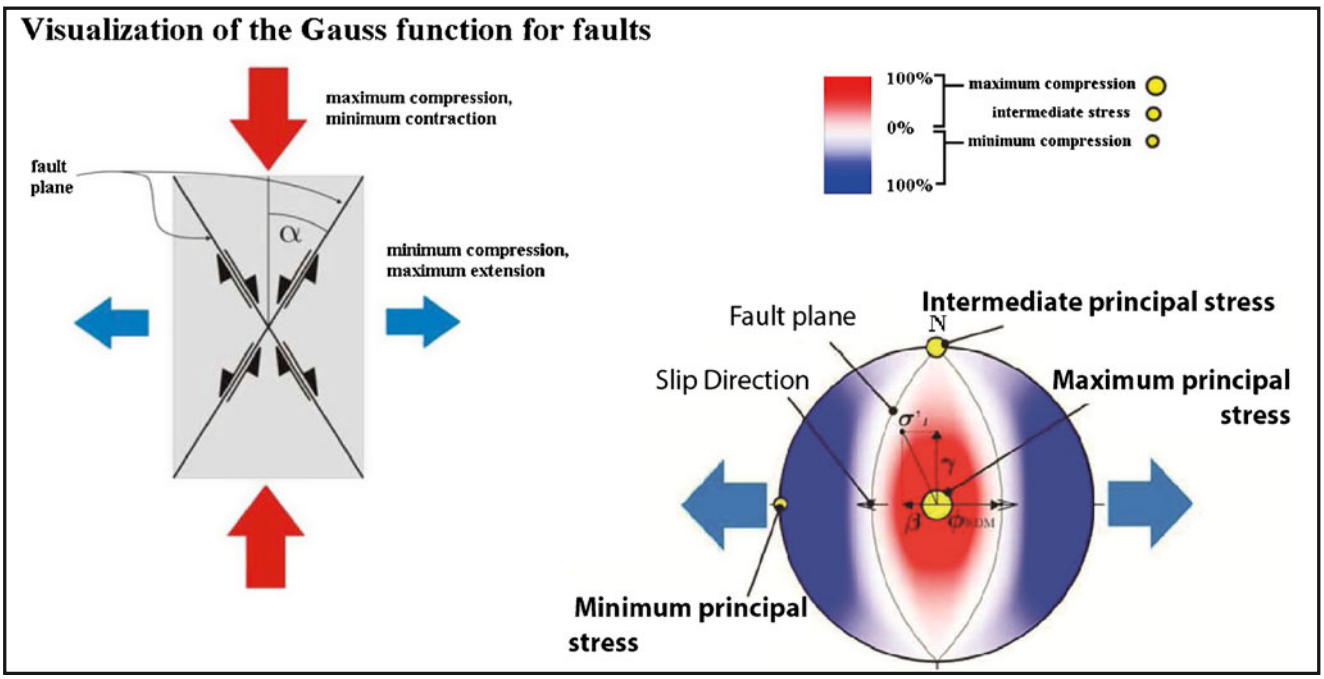

Fig. 4 Legend of the stress tensor obtained in the T-TECTO 3.0 stress ellipsoid construction

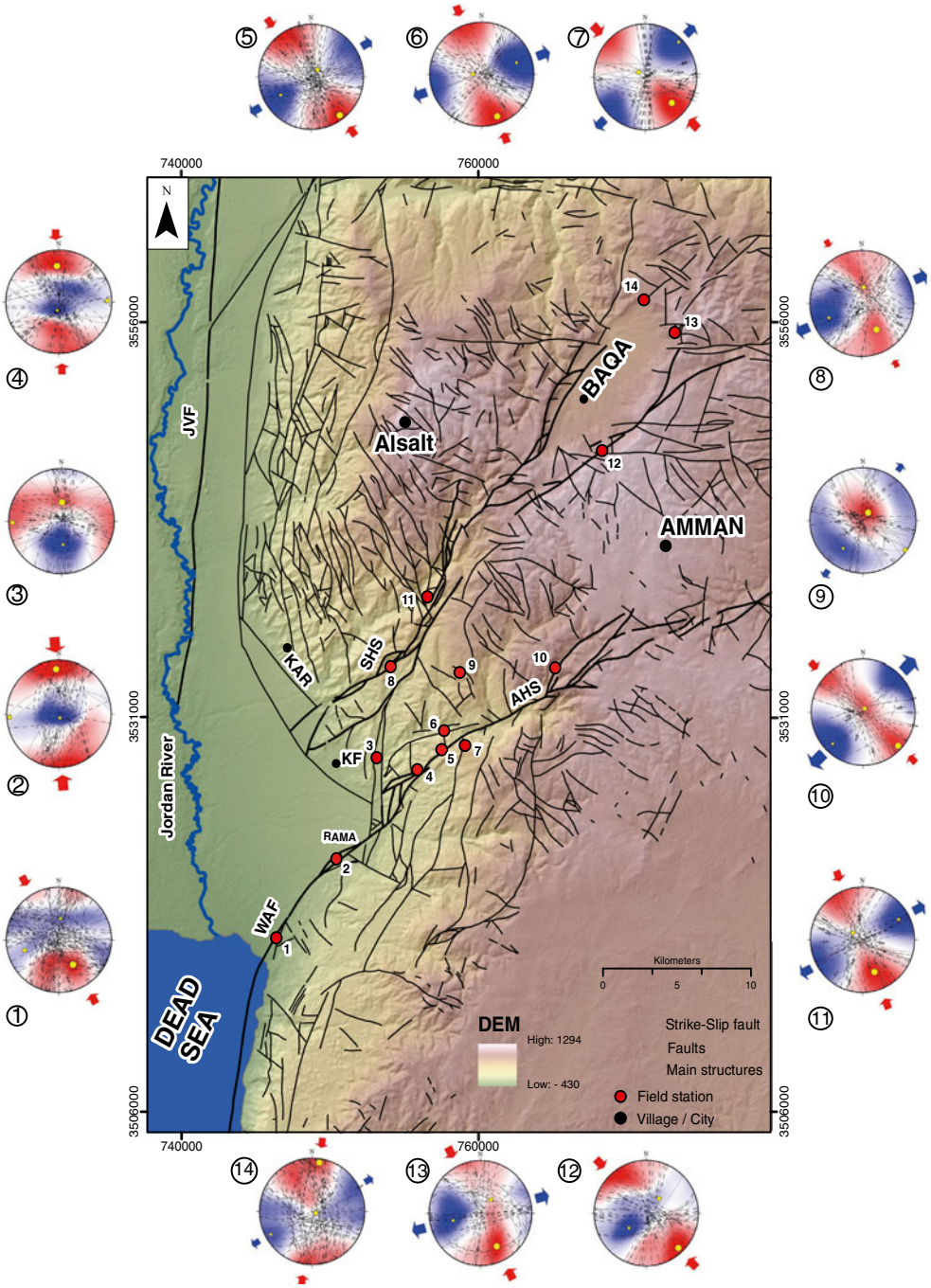

Fig. 5 Stress tensors obtained for the 14 field stations. Locations of the field stations are marked by *red circles* and numbered from 1 to 14. The hillshade base map is derived from 30 m resolution digital elevation model from ASTER GDEM database

stations 2 and 4 (Fig. 5), and normal tensors in stations 3 and 9. Normal tensors were obtained in areas where intense mesoscale normal faulting was identified in the field.

The rose diagram in Fig. 6 illustrates the azimuthal distribution of the maximum stress axis (σ1) in the obtained stress tensors. The azimuth of σ1 lies between N34° and N188°. Although this range is rather large, the 64 % of the stress tensors have a σ1 direction between N 140° and N 180°. This data are quite consistent and indicate a maximum compression in a NNW–SSE direction.

Discussion

Stress analyses of the tectonic structures in the entire DSTF region indicate two different phases of deformation (Zain Eldeen et al. 2002; Diabat et al. 2004; Lunina et al. 2005; Diabat 2009: Hardy et al. 2010; Palano et al. 2013); NNW-SSE compression stress related to present-day stress field and WNW-SES compression stress of Cretaceous age. Diabat (2009) proposed a possible Quaternary activity in the northernmost part of AHS. This study obtained sub-horizontal σ1

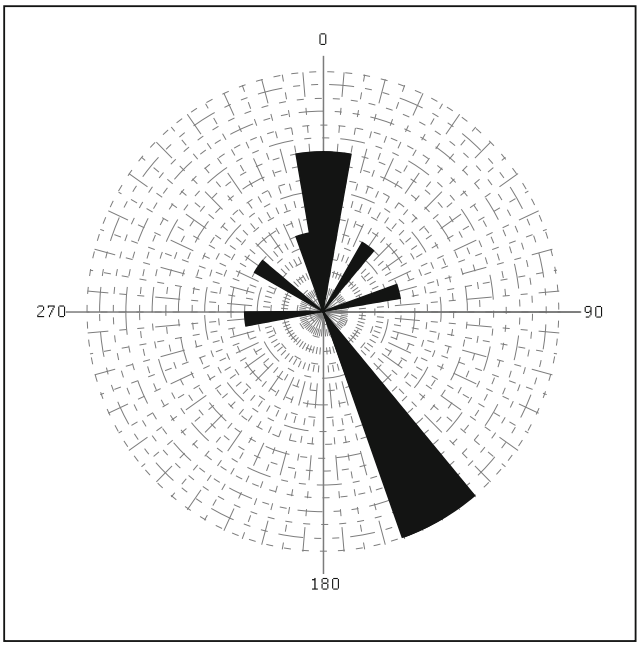

Fig. 6 Rose diagram of the azimuthal distribution of the maximum compressive stress axis (σ1) in the 14 stations

and σ3 and a sub-vertical σ2 in most stress tensors. Thus, a major strike-slip system with σ1 swinging around N to NW direction was dominant in the studied structures. As it has been recognized in previous works (Chaimov et al. 1990; Eyal 1996; Badawy and Horváth 1999; Hofstetter et al. 2007; Eyal and Eyal 2015), we consider that some of the structures at their junction with the DSTF still interact with it.

In this study, we obtained three types of stress tensors from the fault-slip inversion. Most of tensors (10 out of 14) are strike-slip type with a NNW-SSE maximum compressive stress axis with different orientation of σ1 and σ3. Only two tensors show normal deformation, with a sub-vertical σ1 and sub-horizontal σ3 and σ2. Both tensor types are compatible with the present-day tectonic frame of the Dead Sea stress field and the Reidel shear of the studied structures. Moreover, our field observations in the area suggest changes in the stress field of the AHS and the SHS from dextral thrust deformation during the Cretaceous to strike-slip and oblique reverse faulting in Quaternary.

Although reverse faulting characterizes the original movement along the AHS and the SHS, the sinistral component in

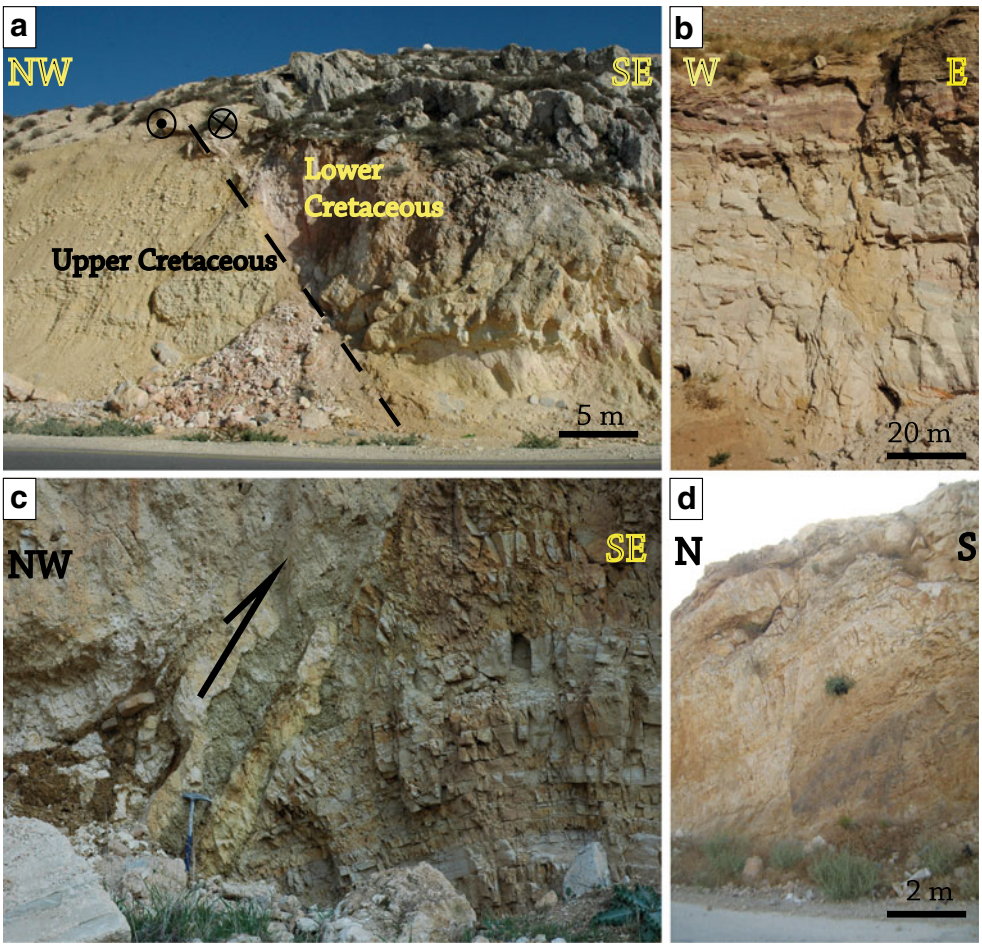

Fig. 7 **a** Oblique sinistral reverse fault NE the Baqa village. **b** Strained layers of the lower Cretaceous sandstone. **c** Left lateral ramp of oblique sinistral-thrust fault to the NE of the Baqa village. **d** Positive half flower structure of reverse fault of lower Cretaceous block (*right*) on a hanging wall of upper Cretaceous (*left*) the location of this outcrop is 7 km to the east of the Kafrain village

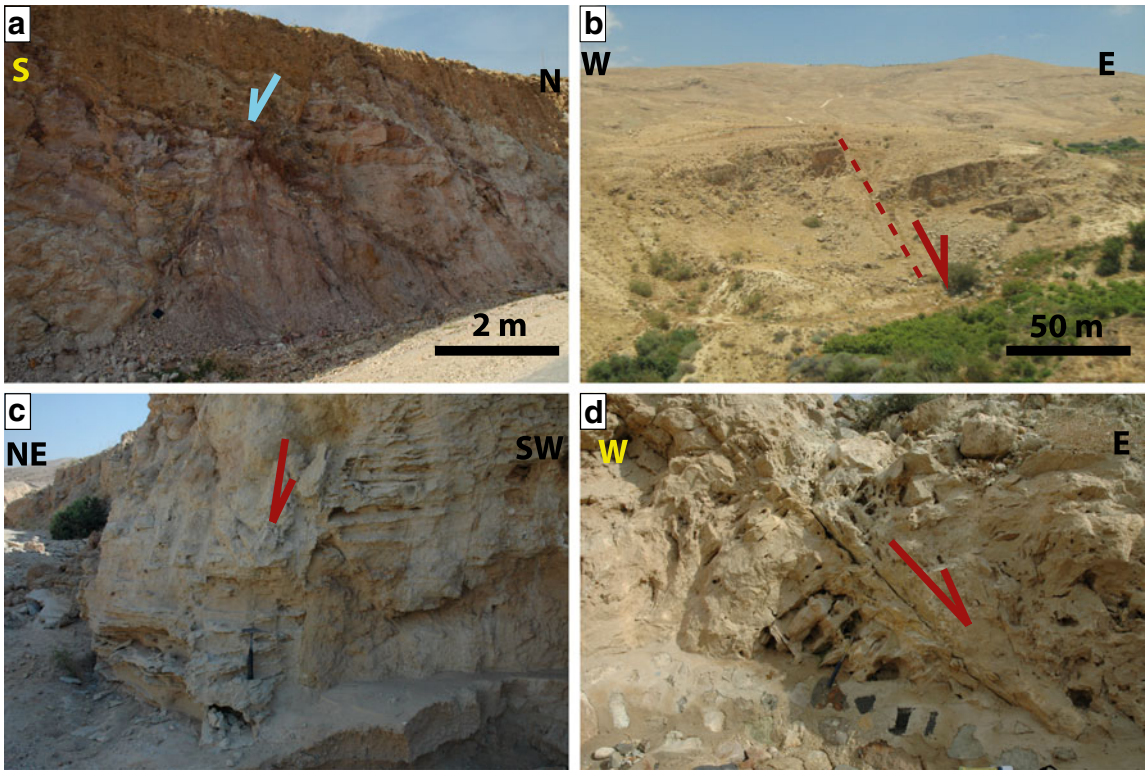

Fig. 8 Different normal faults outcrops in the study area: **a** Lower Cretaceous sandstone 1 km north of the Baqa village. **b** Upper Cretaceous Limestone 6 km NE of the Kafrain village. **c** Lower Cretaceous sandstone 1 km SE of the Rama village. **d** Quaternary travertine 1 km NE from Dead Sea coast

NE orientation was never reported for these structures. During our field works, sinistral movement was documented in all the field stations (Table 1). The kinematics of the tectonic structures in our study area highlights oblique and left-lateral strike-slip movements along the old 30–40° oriented fault planes. Strike-slip and dip-slip kinematic indicators on

Table 2 Max, min, and intermediate compressive stress details and type of tensor

Station no.	δ1		δ2		δ3		Type of tensor
	Direction	Magnitude	Direction	Magnitude	Direction	Magnitude	
1	150/32	52 %	253/20	N/A	5/45	28 %	Strike-slip/reverse component
2	356/9	68 %	266/2	N/A	165/81	62 %	Pure reverse
3	0/50	36 %	268/3	N/A	176/41	72 %	Oblique normal
4	357/19	52 %	89/4	N/A	189/70	51 %	Pure reverse
5	143/4	51 %	43/69	N/A	239/21	56 %	Pure strike-slip
6	160/7	51 %	271/71	N/A	72/18	64 %	Pure strike-slip
7	134/17	58 %	305/72	N/A	45/3	62 %	Pure strike-slip
8	150/29	36 %	7/55	N/A	247/20	66 %	Strike-slip/reverse component
9	34/70	54 %	125/1	N/A	215/23	41 %	Pure normal
10	133/3	45 %	25/80	N/A	225/9	78 %	Pure strike-slip
11	159/22	50 %	306/64	N/A	61/12	58 %	Pure strike-slip
12	308/56	55 %	79/24	N/A	178/20	55 %	Pure normal
13	80/64	66 %	236/24	N/A	333/15	37 %	Pure normal
14	137/5	55 %	42/48	N/A	230/42	58 %	Pure strike-slip
15	153/18	54 %	38/53	N/A	256/31	63 %	Strike-slip/reverse component
16	8/3	43 %	117/81	N/A	241/5	38 %	Pure strike-slip

the fault planes suggest that the faults were re-activated at a later stage.

During faulting, fractures spread in all directions being consistent with the Reidel shear model. This model suggests a NW-SE maximum compressive stress axes and NE-SW minimum compressive strength, similar to the regional stress field configuration (Fig. 1c). According to this model, structures like R2 (normal faults) and X (dextral faults) can occur in the tectonic context of the area. These kinds of faults were found in the central study area between the AHS and the SHS (faults documented in field station no. 3). The X-fault type is abundant in the NW parts of the study area, whereas scarce in the region between the AHS and the SHS. The lack of these faults in this area can be explained by the control of NE sinistral-thrust faults of the AHS and the SHS. The youngest N-S to NNW-SSE compressional stress affected the area and produced the major oblique sinistral reverse fault and its related local structures.

The results of stress analysis based on seismological data (Hofstetter et al. 2007 and Palano et al. 2013) along with the present-day stress analyses (e.g., Lunina et al. 2005; Palano et al. 2013) are consistent and compatible and support the hypothesis that stress axes follow the Anderson model in which two of the principal stresses are horizontal and the third one vertical. For the sites discussed in our work, this criterion is attained. Because 12 out of 14 stress tensors show a NNW–SSE direction of compression compatible with the strike of the regional (σ1) stress, we envisage that they also reflect the driving mechanism of Quaternary active tectonics.

Our results suggest a reactivation of the AHS and SHS in the Neogene and Quaternary times coherent with the present-day stress field of the DSTF. At this respect, the WAF probably is transferring marginal movement to the AHS. The segment connecting the WAF to the AHS could be considered the northernmost part of WAF, although it appears in some works as an eastern boundary fault.

Conclusions

In this work, we presented a structural analysis of fault-slip data collected from the AHS, SHS, and the northernmost termination of the WAF. The fault-slip analysis of these tectonic structures suggests a stress pattern with horizontal σ1 and σ3 axes striking NNW-SSE and NE-SW, respectively. This stress pattern is similar to the one associated with the DSTF. These new findings were corroborated with field data of meso-scale faults in 12 out of 14 sites, thus supporting a Neogene-Quaternary reactivation in the region.

We have presented field evidences of the different faulting mechanisms that affect the AHS and SHS. In both structures, the old dextral-reverse striations were overprinted by newer ones of sinistral reverse and sinistral strike-slip kinematics. These conclusions are compatible with recent studies in the region and can explain the relationship between the WAF and AHS and SHS by means of crustal stress distribution to the NE of the Dead Sea during the Miocene to recent.

Acknowledgments This work has been funded with the research project CGL2011-29920 from the Plan Nacional de Investigación Científica, Desarrollo e Innovación Tecnológica 2008–2011 (Spain), the project Erasmus Mundus External Cooperation Window, Lot 3, and the research grant from Tafila Technical University (Jordan).

References

Abed AM (2000) Geology of Jordan, Jordanian Geologists Association Publications, Amman, p 570 (In Arabic)

Abed AM, Yaghan R (2000) On the paleoclimate of Jordan during the last glacial maximum. Palaeogr Palaeoclimateol Palaeoecol 160:23–33

Abou Romieh M, Westaway R, Doud M, Radwan Y, Yassminh R, Khalil A, Al-Ashkar A, Loughlin S, Arrell K, Bridgland D (2009) Active crustal shortening in NE Syria revealed by deformed terraces of the River Euphrates. Terra Nov. 21:427–437. doi:10.1111/j.1365-3121.2009.00896.x

Alchalbi A, Daoud M, Gomez F, McClusky S, Reilinger R, Abu Romeyeh M, Alsouod A, Yassminh R, Ballani B, Darawcheh R, Sbeinati R, Radwan Y, Al Masri R, Bayerly M, Al Ghazzi R, Barazangi M (2010) Crustal deformation in northwestern Arabica from GPS mesurments in Syria: slow slip rate along the northern Dead Sea Fault. Geophys J Int 180:125–135. doi:10.1111/j.1365-246X.2009.04431.x

Al-Tarazi E, Abu Rajab J, Gomez F, Cochran W, Jaafar R, Ferry M (2011) GPS measurements of near-field deformation along the southern Dead Sea fault system. Geochem Geophys Geosyst 12:Q12021. doi:10.1029/2011GC003736

Angelier J (1989) From orientation to magnitudes in paleostress determinations using fault slip data. J Struct Geol 11:37–50

Angelier J (1990) Inversion of field data in fault tectonic to obtain the regional stress—III. A new rapid direct inversion method by analytical means. Geophys J Int 103:363–376

Angelier J (1994) Fault slip analysis and paleostress reconstruction. In: Hancockm PL (ed) Continental deformation. Pergamon, Oxford, pp 101–120

Atallah M (1992) Tectonic evolution of northern Wadi Araba. Jordan Tectonophysics 204:17–26

Badawy A, Horváth F (1999) The Sinai subplate and tectonic evolution of the northern Red Sea region. J Geodyn 27:433–450

Bott MHP (1959) The mechanism of oblique slip faulting. Geol Mag 96: 109–117

Chaimov TA, Barazangi M, Al-Saad D, Sawaf T, Gebran A (1990) Crustal shortening in the Palmyride fold belt, Syria, and implication for movement along the Dead Sea fault system. Tectonics 9: 1369–1386

Delvaux D (1993) The TENSOR program for paleostress reconstruction: example from the East Africa and the Baikal Rift Zones. In: EUGVII, vol. 5. Strassbourg, France, Terra Nova, p. 216

Delvaux D (2011) Win-Tensor, an interactive computer program for fracture analysis and crustal stress reconstruction. EGU general assembly, Vienna, 2011. Geophys Res Abstr 13:EGU2011–EGU4018

Delvaux D, Moeys R, Stapel G, Melnikov A, Ermikov V (1995) Paleostress reconstructions and geodynamics of the Baikal region, Central Asia. Part 1: Paleozoic and Mesozoic pre-rift evolution. Tectonophysics 252:61–101

Diabat AA (2009) Structural and stress analysis based on fault-slip data in the Amman area, Jordan. J Afr Earth Sci 54:155–162. doi:10.1016/j.jafrearsci.2009.03.011

Diabat AA, Atallah M, Salih MR (2004) Paleostress analysis of the Cretaceous rocks in the eastern margin of the Dead Sea transform, Jordan. J Afr Earth Sci 38:449–460. doi:10.1016/j.jafrearsci.2004.04.002

Eyal Y (1996) Stress fluctuations along the Dead Sea rift since the Middle Miocene. Tectonics 15:157–170

Eyal Y, Eyal M (2015) Nature of slip transfer between strike-slip faults: the eastern sinan (Egypt) shear zone, Dead Sea transform. J Struct Geol 76:52–60. doi:10.1016/j.jsg.2015.03.014

Eyal Y, Gross MR, Engelder T, Becker A (2001) Joint development during fluctuation of the regional stress field in southern Israel. J Struct Geol 23:279–296

Ferry M, Meghraoui M, Abou Karaki N, Al-Taj M, Amoush H, Al-Dhaisat S, Barjous M (2007) A 48-Kyr-long slip rate history for the Jordan valley segment of the Dead Sea fault. Earth Planet Sci Lett 260:394–406. doi:10.1016/j.epsl.2007.05.049

Garfunkel Z (1981) Internal structure of the Dead Sea leaky transform (rift) in relation to plate kinematics. Tectonophysics 80:80–108

Gòmez F, Karam G, Khawalie M, McClusky S, Vernant P, Reilinger R, Jaffar R, Tabet C, Khair K, Barazangi M (2007) Global positioning system measurements of strain accumulation and slip transfer through the restraining bend along the Dead Sea fault system in Lebanon. Gephys J Int 168:1021–1028. doi:10.1111/j.1365-246X.2006.03328.x

Hardy C, Homberg C, Eyal Y, Barrier E, Muller C (2010) Tectonic evolution of the southern Levant margin since _Mesozoic. Tectonophysics 494:211–225. doi:10.1016/j.tect.2010.09.007

Hasse-Schramm A, Goldstein S, Stein M (2004) U-Th dating of Lake Lisan (Late Pleistocene Dead Sea) aragonite and implications glacial East Mediterranean climate change. Geochim Cosmochim Acta 68(5):985–1005. doi:10.1016/j.gca.2003.07.016

Hofstetter R, Klinger Y, Amrat AQ, Rivera L, Dorbath L (2007) Stress tensor and focal mechanisms along the Dead Sea fault and related elements based on seismological data. Tectonophysics 429:165–181. doi:10.1016/j.tecto.2006.03.010

Homberg C, Bachmann M (2010) Evolution of the Levant margin and western Arabia platform since the Mesozoic: introduction. Geological society, vol 341. Special Publication, London, pp 1–8. doi:10.1144/SP341.1

Klinger Y, Avouac JP, Abou Karaki N, Dorbath L, Bourles D, Reyes JL (2000) Slip rate on the Dead Sea transform fault in the northern Araba valley (Jordan). Geophys J Int 142:755–768

Landmann G, Abu Qudaira GM, Shawabkeh K, Wrede V, Kempe S (2002) Geochemistry of the Lisan and Damya formations in Jordan and implications for palaeoclimate. Quat Int 89:45–57

Le Beon M, Klinger Y, Amrat AQ, Agnon A, Dorbath L, Baer G, Ruegg JC, Charade O, Mayyas O (2008) Slip rate and locking depth from GPS profiles across the southern Dead Sea transform. J Geophys Res 113:B11403. doi:10.1029/2007JB005280

Le Beon M, Klinger Y, Al-Qaryouti M, Mériaux AS, Finkel RC, Elias A, Mayyas O, Ryerson FJ, Tapponnier P (2010) Early Holocene and late Pleistocene slip rates of the southern Dead Sea fault determined from 10Be cosmogenic dating of offset alluvial deposits. J Geophys Int 115:B11414. doi:10.1029/2009JB007198

Lunina OV, Mart Y, Gladkov AS (2005) Fracturing patterns, stress fields and earthquakes in the Southern Dead Sea rift. J Geodyn 40:216–234. doi:10.1016/j.jog.2005.07.010

Makhlouf IM (2003) Fluvial/tidal interaction at the southern Tethyan strandline during Triassic Mukheiris times in central Jordan. J Asian Earth Sci 21:377–385

Masri M (1963) Report on the geology of the Amman-Zarqa area. Central Water Authority, Amman, Unpublished report, 74 p

McClusky S, Reilinger R, Mahmoud S, Ben Sari D, Tealeb A (2003) GPS constraints on Africa (Nubia) and Arabia plate motions. Geophys J Int 155:126–138

Mikbel S (1986) Some relevant tectonical and geotechnical considerations of south Amman area/Jordan. Dirasat 7:215–225

Mikbel S, Zacher W (1981) The Wadi Shueib structure in Jordan. N Jaharbuch Geol Paleontol Monat 9:215–225

Palano M, Imprescia P, Gresta S (2013) Current stress and strain-rate fields across the Dead Sea fault system: constraints from seismological data and GPS observations. Earth Planet Sci Lett 369–370:305–316. doi:10.1016/j.epsl.2013.03.043

Powell JH (1989) Stratigraphy and sedimentation of the phanerozoic rocks in Central and South Jordan. 1–50000 geological mapping series, national resources authority. Geol Bull 11:1–130

Quennell AM (1959) Tectonics of the Dead Sea Rift. 20th Internacional Congreso Geólogo. Asociación y Servicios Geólogos Africanos. pp 385–403

Reilinger R, McClusky S (2011) Nubia-Arabia-Eurasia plate motions and the dynamics of Mediterranean and Middle East tectonics. Geophys J Int 186:971–979. doi:10.1111/j.1365-246X.2011.05133.x

Wallace RE (1951) Geometry of shearing stress and relation to faulting. J Geol 59:118–130

Zain Eldeen U, Delvaux D, Jacobs P (2002) Tectonic evolution in the Wadi Araba Segment of the Dead Sea Rift, South-West Jordan. EGU Stephan Mueller Spec Publ Ser 2:63–81

Zalohar J (2009) T-TECTO 3.0 Professional: integrated software for structural analysis of fault-slip data. Introductory Tutorial. The software was downloaded from http://www2.arnes.si/~jzaloh/t-tecto_homepage.htm

Zalohar J (2012) Cosserat analysis of interaction between intersecting faults: the wedge faulting. J Struct Geol 37:105–123. doi:10.1016/j.jsg.2012.01.023

Zalohar J, Verbac M (2007) Paleostress analysis of heterogenous fault-slip data: the Gauss method. J Struct Geol 29:1798–1810. doi:10.1016/j.jsg.2007.06.009